RSC Advances

PAPER

View Article Online
View Journal | View Issue

Cite this: *RSC Adv.*, 2022, **12**, 32318

Eu- and Tb-adsorbed Si_3N_4 and Ge_3N_4: tuning the colours with one luminescent host†

Cordula Braun, *[a] Liuda Mereacre,[a] Zheng Chen,[b] Adam Slabon,[c] David Vincent,[d] Xavier Rocquefelte[d] and Jean-François Halet[e]

Received 26th July 2022
Accepted 1st November 2022

DOI: 10.1039/d2ra04663f

rsc.li/rsc-advances

Phosphor-converted white light emitting diodes (pc-LEDs) are efficient light sources for applications in lighting and electronic devices. Nitrides, with their wide-ranging applicability due to their intriguing structural diversity, and their auspicious chemical and physical properties, represent an essential component in industrial and materials applications. Here, we present the successful adsorption of Eu and Tb at the grain boundaries of bulk β-Si_3N_4 and β-Ge_3N_4 by a successful combustion synthesis. The adsorption of europium and terbium, and the synergic combination of both, resulted in intriguing luminescence properties of all compounds (red, green, orange and yellow). In particular, the fact that one host can deliver different colours renders Eu,Tb-β-M_3N_4 (M = Si, Ge) a prospective chief component for future light emitting diodes (LEDs). For the elucidation of the electronic properties and structure of β-Si_3N_4 and β-Ge_3N_4, Mott–Schottky (MS) measurements and density functional theory (DFT) computations were conducted for the bare and RE adsorbed samples.

Main

Phosphor-converted white light-emitting diodes (pc-LEDs) are emerging as an indispensable solid-state light source for the next generation lighting industry and display systems due to their unique properties.[1,2]

Doped gallium nitride (GaN) has been the benchmark in the past decades in this domain and has indeed driven the LED revolution in lighting and displays as a key material. The concept of down-conversion of a GaN-based blue LED, being awarded the Nobel prize in 2014 in physics,[3–5] offers the possibility to provide efficient generation of monochromatic, high-colour purity light resulting in a highly efficient warm-white all-nitride phosphor-converted light emitting diode (pc-LED). The combination of the lower energy consumption, high light quality, preservation of colour point stability and long lifetime is one of the key benefits of pc-LEDs, having the potential to reduce global energy consumption in the lighting sector substantially.

Silicon nitride (Si_3N_4) high performance ceramics are used in numerous applications because of their superior mechanical properties.[6,7] The wide-ranging applicability of nitrides and their related (oxo)nitridosilicate family can be ascribed to their significantly extended structural varieties as well as their auspicious chemical and physical properties (very high chemical and thermal stability, very high quantum efficiency, very low thermal quenching).

In particular, Eu^{2+}-doped (oxo)nitridosilicates and SiAlONs have been amply studied as important host lattices for phosphor-converted light-emitting diodes (pc-LEDs).[8–25]

For instance, $M_2Si_5N_8$:Eu^{2+} (red-orange, 2-5-8 phosphor) and $MSi_2O_2N_2$:Eu^{2+} (yellow-green, 1-2-2-2 phosphor) (M = Ca, Sr, Ba) were significant discoveries in this field. Several Mg-nitridosilicates and nitridoaluminates were also developed as next generation high efficient red emitting phosphor materials with superior luminescence properties.[26–30]

The next step in phosphor development is the investigation of novel host materials for narrow-band emitting phosphors to enhance luminous efficacy and improving therefore the quality of light emitting diodes (LEDs) for diverse applications upon doping.

Silicon nitride (Si_3N_4) materials have been found to meet these requirements due to its rigid lattices with highly covalent network and high thermal stability.[31,32] However, looking at the literature indicates that there are only a few investigations concerning rare-earth doped silicon nitride materials. In most cases only Eu- and Tb-doped α-Si_3N_4 thin films and nanowires illustrating broad band emission are concerned.[33–41] Here we

[a]*Karlsruhe Institute of Technology (KIT), Institute for Applied Materials (IAM), Herrmann-von-Helmholtz-Platz 1, D-76344 Eggenstein-Leopoldshafen, Germany. E-mail: Cordula.Braun@kit.edu*

[b]*Institute of Inorganic Chemistry, RWTH Aachen University, Landoltweg 1, D-52056 Aachen, Germany*

[c]*Chair of Inorganic Chemistry, University of Wuppertal, Gaussstr. 20, 42119 Wuppertal, Germany*

[d]*Univ. Rennes – CNRS, Institut des Sciences Chimiques de Rennes, UMR 6226, 35042 Rennes, France*

[e]*CNRS – Saint-Gobain – NIMS, IRL 3629, Laboratory for Innovative Key Materials and Structures (LINK), National Institute for Materials Science (NIMS), 1-1 Namiki, Tsukuba 305-0044, Japan*

† Electronic supplementary information (ESI) available. See DOI: https://doi.org/10.1039/d2ra04663f

use the expression doping explicitly as this is given in the references.

There are many works in the literature regarding the influence of rare-earth oxides additives often defining the morphology of β-Si_3N_4 crystallites growing in a multiphase ceramic, thereby affecting its microstructure and mechanical toughness of the ceramic.[42–49] Densification additives (*e.g.*, rare-earth (RE) oxides) play an important role in the fabrication of silicon nitride-based ceramics. Indeed, the affinity of the RE cations to segregate and adsorb on the prismatic planes of the hexagonal grains in β-Si_3N_4, exhibiting very anisotropic shapes, is used to develop microstructural features (*e.g.*, the initiation of the α,β-transformation and the formation of elongated reinforcing grains) required for particular applications.[43]

Phosphors are usually doped with Eu^{2+} and only one activator ion is used. Therefore, one host shows one colour. The fact that nitride bulk material can be doped with several rare-earth activator ions, even at the same time, is absolutely new resulting in the fact that one host can deliver different colours.

As well novel is the fact that a pure nitride host material shows green luminescence,[31,32] till now this could only be realized by oxynitrides and oxonitridosilicates.[18,50–53]

Just recently we demonstrated that the so called "yellow gap" could be closed for bulk GaN *via* co-doping with europium and terbium.[32] Co-doping really opens up a multitude of degrees of freedom to customize and adapt a luminescent material to specific needs.

Herein, we experimentally and theoretically examine the adsorption of Eu and Tb at the grain boundaries of β-Si_3N_4 and β-Ge_3N_4 and discuss their resulting intriguing luminescence properties.

At this point we would like to point out that we explicitly talk here of adsorption of the RE elements and not of doping. In the nitridosilicate $Ca_2Si_5N_8$:Eu^{2+} the RE cations go the Ca site of the host structure, which is named doping. But there is no analogous cation site in β-Si_3N_4 and β-Ge_3N_4.

As described in detail in literature[43,44,49] the RE cations go to the grain boundaries in β-Si_3N_4. Therefore we choose the term Eu adsorbed-Si_3N_4 and not doped as it is used for *e.g.* Eu-doped nitridosilicates. For a detailed discussion concerning this topic we would like to refer to lit.[43,44,49] and the section below, where a detailed explanation of the RE adsorption sites is given.

(For β-Si_3N_4 and β-Ge_3N_4 adsorbed with europium and/or terbium we would like to introduce the notation Eu,Tb-β-M_3N_4.) The results indicate that Eu,Tb-β-Si_3N_4 (ref. 31) and as well as Eu,Tb-β-Ge_3N_4 (ref. 31) should be considered as prospective chief components for highly efficient warm-white all-nitride phosphor-converted light emitting diode (pc-LED).

Results

Structure and composition characterization

A low temperature urea-based synthetic approach was successfully used to combine β-Si_3N_4 and β-Ge_3N_4 (Chempur 99 999%) with $MCl_3 \cdot x6H_2O$ or $M(NO_3)_3 \cdot x5H_2O$ (M = Eu, Tb). (see Fig. 1a and S1–S3†).[31]

For a comparison of the powder diffraction patterns of Eu-β-Si_3N_4 and Tb-β-Si_3N_4 see Fig. S1,† for Tb-β-Ge_3N_4 and Eu,Tb-β-

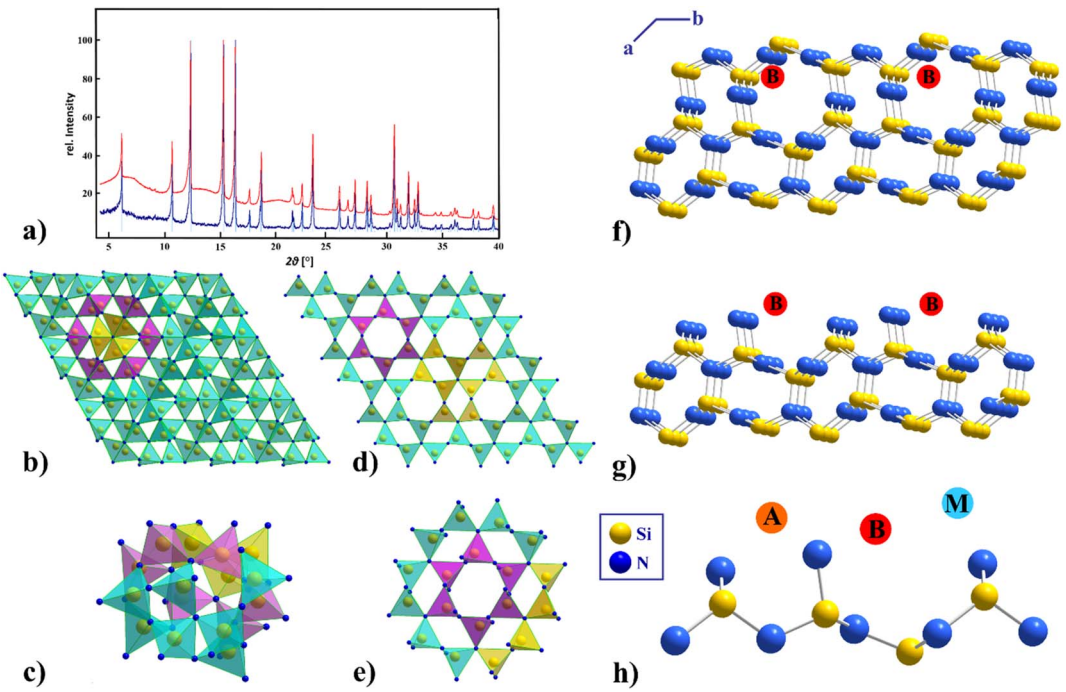

Fig. 1 (a) X-ray powder diffraction patterns of pure β-Si_3N_4 (blue), adsorbed Eu-β-Si_3N_4 (red) and the bar graph of β-Si_3N_4 ICSD [33-1160] (bright blue), ($\lambda = 0.709026$ Å), (b) structure of α-Si_3N_4 view along [001], (c) cavity for a possible insertion of a RE cation in α-Si_3N_4, (d) structure of β-Si_3N_4 view along [001], (e) six-ring representation of β-Si_3N_4, (f, g and h) structure of β-Si_3N_4 view along [001] with three possible RE adsorption sites A, B, and M.[44] (Si atoms are depicted in yellow, N atoms in blue, the RE adsorption sites A, B, and M in orange, red and light blue).

Ge_3N_4, see Fig. S3.† SEM EDX measurements of β-Si_3N_4 and β-Ge_3N_4 confirmed the atomic ratio of M : N (M = Si, Ge) of 3 : 4 and europium and terbium contents of 3–5% were found (see Fig. S4†).

Understanding the influence of selective dopant additions and the role of interfacial interactions is central to the design of novel high-performance Si_3N_4 ceramics by offering the potential for customizing the materials properties. Rare-earth cations are often located within regions of the oxynitride glassy phase of triple-junction pockets, disordered amorphous nanometer scale intergranular films (IGF) and at the glass or IGF/β-Si_3N_4 grain interfaces.[44]

According to the literature[44,49] there are three independent stable RE adsorption sites per surface unit cell along the N-terminated prismatic planes of β-Si_3N_4 (see Fig. 1f–h). A and B are stable RE equilibrium sites, while calculations pretended the M site to be theoretically unstable, although observed experimentally in the case of La adsorption.[44] Stereochemical bonding factors are found to determine the adsorption site preferences contrary to ionic size effects, and the strength of the rare-earth interface bonding is defined *inter alia* by the electronic structure of the nitride surface. Shibata *et al.*[49] showed that these RE adsorption sites have higher binding energies than Si, partially reside on cation sites normally only available for Si and that the RE–N bonds are longer than comparable Si–N bonds. While in β-Si_3N_4 an adsorption of the RE ions at the grain boundaries is possible (see Fig. 1f–h), in α-Si_3N_4 an insertion of cations into the structure (see Fig. 1c) takes place. In the α-Si_3N_4 structure there are two caves (for the bigger one see Fig. 1c), which can be occupied when charge is balanced by cation and/or anion substitutions (*e.g.*, Si by Al and N by O). This additional insertion of an RE ion is stabilizing the α-Si_3N_4, which is otherwise metastable.[54] And indeed, no insertion of cations is realized into the six rings in β-Si_3N_4 (see Fig. 1e).

Luminescence properties

One of the most important activator ions with red emission is Eu^{3+} corresponding to the transition $^5D_0 \rightarrow {}^7F_J$ (J = 1–6). For Tb^{3+}, the green emission is due to the transition between the ^5D_J emitting states and the ^7F_J ground states, where the main intense green emission is attributed to the $^5D_4 \rightarrow {}^7F_5$ transition (544 nm).

An important point here is that normally the RE ion of luminescent phosphors is inserted during the main synthesis and not afterwards. In general, doping of nitridosilicates is performed with Eu^{2+} and only one activator ion is used for one luminescent host. Blending the colours within one host and colour tuning by mixing different coloured luminescent hosts should open up tremendous opportunities for highly efficient phosphors. Within the scope of this work, β-Si_3N_4 and β-Ge_3N_4 were adsorbed with Eu and Tb activator ions each individually and both simultaneously.

In the CIE 1931 diagram (see Fig. 2e) the chromaticity coordinate positions of Eu- and Tb-β-Si_3N_4 and β-Ge_3N_4 are indicated, proving that a colour tuning of one host with different activator ions and their combination is feasible.

Taking into account the basics of colour mixing, it is clear that the combination of green and red leads to orange (see Fig. 2f). This effect could be proven in the meantime for other doped nitrides[31] *e.g.*, GaN[31,32] (see Fig. 2e), and carbodiimides as well.[55]

Adsorption of β-Si_3N_4 and β-Ge_3N_4 with europium

Eu-β-Si_3N_4 and Eu-β-Ge_3N_4 show strong characteristic emission peaks of Eu^{3+} within the region of 570–705 nm, indicating an energy transfer between the β-Si_3N_4 and β-Ge_3N_4 hosts and the Eu^{3+} ions. The peaks associated with the intra-4f shell transitions ($^5D_0 \rightarrow {}^7F_J$) of the Eu^{3+} ions, are found at 577, 594, 612, 614, 619, 646 and 700, 705 nm, with those at 612 and 614 nm the most intense ones for β-Si_3N_4 (see Fig. 2a) whereas for Ge_3N_4, the corresponding peaks are located at 577, 593, 613 (the most intense), 646 and 700 nm (see Fig. 2b).

Fig. 2a shows that in the emission spectrum of Eu-β-Si_3N_4, the transitions $^5D_0 \rightarrow {}^7F_0$ and $^7F_3$ seem to be more intense than usually, and the latter is even more pronounced than the $^5D_0 \rightarrow {}^7F_4$ transition, which is not common. This means a strong *J*-mixing and a strong crystal-field perturbation might occur in this matrix. The peak corresponding to the $^5D_0 \rightarrow {}^7F_0$ transition is also broad, indicating the location of Eu^{3+} ions on several sites in the host structure (see Fig. 2a).

Adsorption of β-Si_3N_4 and β-Ge_3N_4 with terbium

The excitation (monitored at 544 nm) and emission spectra of Tb-β-Si_3N_4 and Tb-β-Ge_3N_4 are represented in Fig. 2c and d. The excitation spectrum of Tb-β-Si_3N_4 and Tb-β-Ge_3N_4 exhibit a broad and intense band in the range from 280 nm to 380 nm with peaks at around 342 and 356 nm, respectively. This broad band is attributed to $4f^8 \rightarrow 4f^75d^1$ transition of the Tb^{3+} ions. The strongest emission peak is at 544 nm with a full width at half maximum (FWHM) ~12 nm corresponding to the $^5D_4 \rightarrow {}^7F_5$ transition, while the peaks at 488, 489 nm, 584 nm and 620 nm originate from the $^5D_4 \rightarrow {}^7F_6$, $^5D_4 \rightarrow {}^7F_4$ and $^5D_4 \rightarrow {}^7F_3$ transitions of the Tb^{3+} ions, respectively. The green luminescence of Tb-β-Si_3N_4 and Tb-β-Ge_3N_4 demonstrates impressively that green emitting phosphors[31] can be also achieved with purely nitride compounds and not only with oxynitrides (*e.g.*, β-SiAlON:Eu^{2+} [56] or oxonitridosilicates (*e.g.*, $SrSi_2O_2N_2$:Eu^{2+} [57,58] as it was up to now. The energy level distributions of Tb^{3+} and Eu^{3+} ions show a large overlap and their energy transfer has been proven to be very effective.[59] The blue-green light of the Tb^{3+} transition ($^5D_4 \rightarrow {}^7F_{6,5}$) is emitted by polychromatic relaxation and the energy is transferred to the $^5D_1$ and $^5D_0$ levels of the Eu^{3+} by cross relaxation. The Eu^{3+} ions absorbing the energy from Tb^{3+}emit therefore orange light.

Fig. 2f–c proves that for Eu,Tb-Ge_3N_4 two different activator ions can be adsorbed in one host showing the typical bands of Eu^{3+} as well as the ones of Tb^{3+} in one spectrum resulting in a saturated orange body colour. However, this is not only a superposition of the Eu^{3+}- and the Tb^{3+}-spectrum of β-Ge_3N_4 because peak form, intensity and wavelength of this orange spectrum differ clearly in comparison to the spectra of the single doped materials. Therefore, this orange colour is only possible by mixing the ions at an atomic scale and cannot be

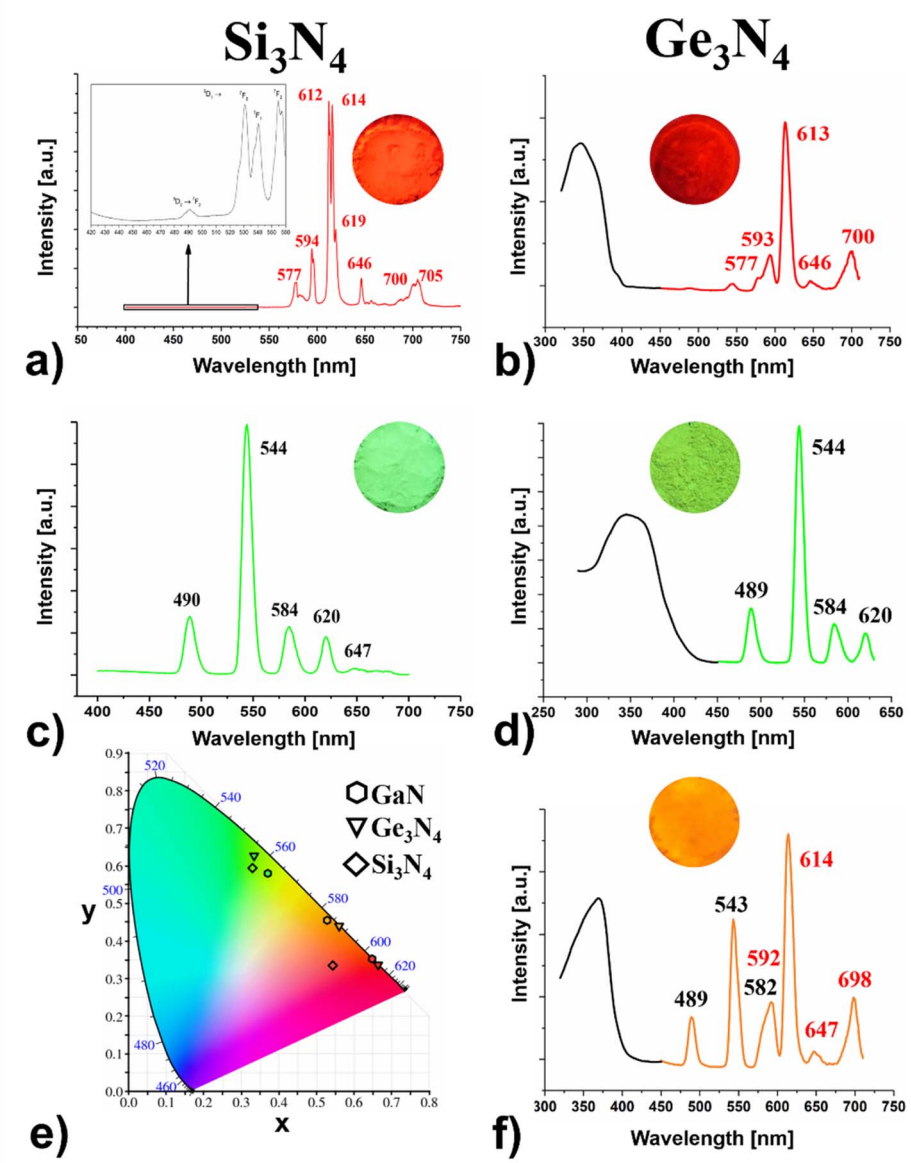

Fig. 2 Excitation (black) and emission spectra (coloured) of (a) Eu-β-Si_3N_4 (red, $\lambda_{em} = 612/614$ nm), (c) Tb-β-Si_3N_4 (green $\lambda_{em} = 544$ nm) and of (b) Eu-β-Ge_3N_4 (red, $\lambda_{em} = 613$ nm), (d) Tb-β-Ge_3N_4 (green $\lambda_{em} = 544$ nm) and (f) Eu- and Tb-β-Ge_3N_4 (orange $\lambda_{em} = 544/614$ nm), (e) CIE 1931 diagram of β-Si_3N_4 (◆), β-Ge_3N_4 (▼) and GaN (●)[31,32] adsorbed/doped with Eu, Tb and Eu and Tb.

realized simply by a mixture of particles of the red and the green adsorbed Ge_3N_4.

To get further evidence powder samples of Eu-Ge_3N_4 and Tb-Ge_3N_4 (same molar ratio Eu : Tb as in Eu,Tb-Ge_3N_4) were mixed in a mortar. This definitely did not result in an orange luminescent β-Ge_3N_4 sample but a yellow luminescent powder instead (see Fig. S5c and d†). Indeed, compared to a superposition of the Eu- and Tb-spectra, all peaks of the Eu,Tb-β-Ge_3N_4 spectrum slightly changed in energy and intensity with the peaks resulting from Tb^{3+} significantly stronger and tuning the colour to the yellow region (CIE coordinates $x, y = 0.456, 0.499$). This clearly evidenced that the orange body colour (CIE values $x, y = 0.559, 0.438$) can only be obtained by an atomic scale mixing and that we are able to tune the colour resulting finally in red, green, orange and yellow luminescence for Eu- and Tb-β-Ge_3N_4. As the mixing at the atomic scale for Eu,Tb-β-Si_3N_4 was not successful, the combination of the powder samples of equal parts of Eu-β-Si_3N_4 and Tb-β-Si_3N_4 was tested. Here we got a completely different result and the CIE diagram shows a saturated orange colour with the coordinates $x, y = 0.570, 0.417$. (see Fig. S5a and b†). Here we find nearly the same CIE values as the ones of the amber emitting 2-5-8 nitridosilicate phosphor $(Ba,Sr)_2Si_5N_8:Eu^{2+}$ ($x, y = 0.579, 0.416$) being considered as an important breakthrough for bridging the "yellow gap".[25]

For Eu,Tb-β-Ge_3N_4 the FWHM pointed out the same value as those of the single doped materials which are in the range of 11–12 nm. This holds true for Tb-β-Si_3N_4 as well. A much more

narrow band is observed for Eu-β-Si_3N_4 with a FWHM of 2–4 nm. Interestingly, these values are quite smaller than the line widths (FWHM) of the emission spectra of the very narrow-band nitridosilicate phosphors which range between 35–50 nm[2] or those of the nitride-based LEDs which vary typically between 20–35 nm.[60] The quantum yields were in the range of 5–16%. Tb-β-Si_3N_4 was 16% and the other compounds around 5%.

To elucidate if the luminescence does not result from the respective rare-earth (RE) compounds and if the Eu and Tb ions really have been adsorbed at the grain boundaries of β-Si_3N_4 and β-Ge_3N_4 a comparison of the luminescence spectra of Eu-Si_3N_4 and Ge_3N_4 and $EuCl_3 \cdot x6H_2O$ is shown in Fig. S6 and S7.† A comparison between Tb-β-Si_3N_4 and TbOCl[61] is also shown in Fig. S15.† Optical and luminescence spectra are highly sensitive to structural deformation of the nearest environment of RE ions. Therefore, it becomes clearly evident here that the emission spectrum has changed due to the adsorption of the Eu cations into the β-Si_3N_4 and β-Ge_3N_4 structures.

A very detailed comparison of our results with those of several Eu- and Tb-Si_3N_4 thin films and nanowires and possible side products published in the literature was carried out (see ESI Fig. S8–S15† and corresponding section). This indicated that if some luminescence spectra may seem very similar overall at first sight, it turns out that definitely some changes are observed.[33–41]

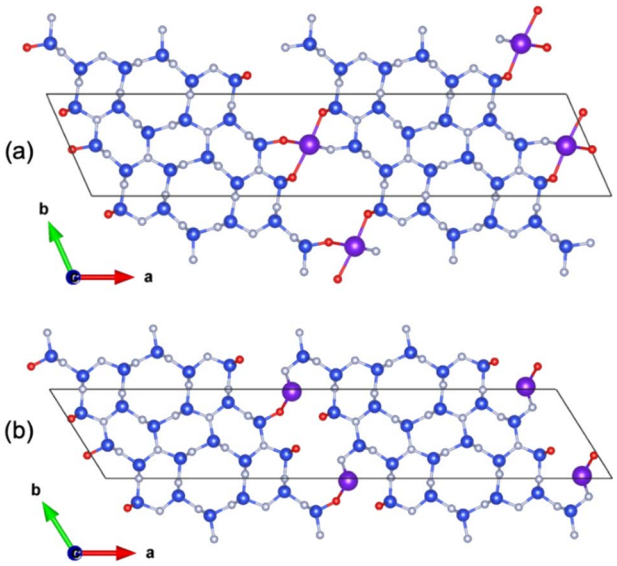

Fig. 3 Relaxed atomic structure for the models used to describe the β-Si_3N_4 grain interface with RE elements (Eu or Tb) at the A-site (a) and B-site (b). Nitrogen, oxygen, hydrogen and RE atoms are represented in blue, red, white and purple, respectively.

DFT calculations

The underlying structure–property relationships in a phosphor, *i.e.*, the relationship between, the nature of the specific atoms, their coordination environment, and the density of states are largely determined by its electronic structure.[62] Therefore, DFT calculations were carried out to further elucidate the adsorption of RE ions at the grain boundaries.

The β-Si_3N_4 models were generated in such a way to reproduce the interface observed in high-angle annular dark-field STEM (HAADF-STEM) images of RE doped Si_3N_4 by Ziegler *et al.*,[63] which evidenced a grain orientated along the [0001] zone axis with the prismatic plane of Si_3N_4 facing the amorphous intergranular phase. In particular, the rare earth elements have been observed sitting on two atomic sites at the interface, labeled A and B, which are, respectively, small and large open hexagonal rings Fig. 3.

Note that the creation of the interface led to dangling bonds, which were passivated using both O^{2-} and N^{3-} ions, in order to respect the electroneutrality of the unit cell. For both Eu and Tb ions on sites A and B, atomic coordinates were relaxed leading systematically to a higher stability when the rare earth resides on site A (highly coordinated) than on site B, with an energy difference of 745 and 851 meV per rare earth for Eu^{3+} and Tb^{3+}, respectively.

For the more stable interface, *i.e.*, with the rare earth located on site A, simulations of the Si L_{23} edge were performed for silicon atoms close to the interface in order to probe both their location and chemical environment. Indeed, precise electron energy loss spectroscopy (EELS) measurements were reported for RE doped Si_3N_4 ceramics,[63] allowing us to compare our model with experimental data. Such a simulation required to properly treat the electron–hole interaction (excitonic effects) using Bethe–Salpeter equations for instance. Here, due to the size of the system, we chose to consider this electron–hole Coulomb interaction as a static screening using the core–hole approximation. More precisely, half an electron was removed from a core orbital, *i.e.*, the Slater's transition state.[64] For the doped Tb-β-Si_3N_4 model, the core-hole was introduced in the $2p_{1/2}$ and $2p_{3/2}$ states of the excited silicon atoms. The simulation is thus a summation of two spectra resulting from two static calculations with, respectively, half a core-hole in $2p_{1/2}$ and $2p_{3/2}$ states of the probed silicon atoms. In order to validate such a static screening approximation, the related bulk system Si_2N_2O was simulated and compared to experiments[63] (see Fig. 4a). A good agreement is observed, with a small discrepancy around 104 eV both in terms of peak position and intensity. Such an agreement confirms that the Slater's transition state allows to properly describe the Si L_{23} edge of silicon atoms surrounded by nitrogen and oxygen atoms.

Fig. 4b shows two simulations corresponding to Si L_{23} edge of two silicon atoms nearby the interface with Tb ions on site A. One silicon atom, labeled Si_1 (Fig. 4b) is surrounded only by nitrogen atoms while the other one, labeled Si_2 (Fig. 4b) is environed by oxygen and nitrogen atoms. Note that the experimental spectrum (open circles) related to site A is characterized by a double peak (102 and 103.5 eV), with a first peak assigned to Si–N bonds and the second one to Si–O bonds. Interestingly, our simulations evidenced a peak at 103 eV for Si_1 and 104.1 eV for Si_2, confirming the previous interpretation and validating the model used to mimic locally the interface in the grain boundary region.

DFT + *U* + SOC calculations were then carried out on the adsorbed Tb-β-Si_3N_4 model considering the previously optimized atomic structures. Such calculations were indeed not trivial and

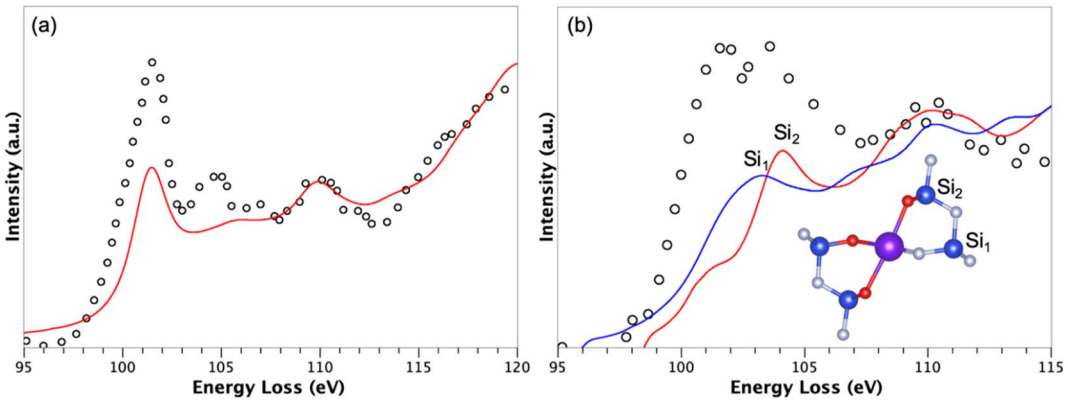

Fig. 4 Simulated Si L_{23} EELS data (red and blue lines) compared to measurements (open circles) from ref. 63 of (a) Si_2N_2O and (b) the adsorbed Tb-β-Si_3N_4 model with Tb ions on A site. The simulations have been done using the Slater's transition state. For the interface, two simulations have been done for one silicon atom surrounded by N^{3-} ions only, and one silicon atom with O^{2-} ions in its first coordination sphere.

could be difficult to converge when the ground state is close in energy to other magnetic states. The convergence of these calculations was achieved only for the Tb compounds. Spin (orbital) moments of 6.03 (1.45) and 6.04 (2.73) μ_B were computed for Tb ions on sites A and B, respectively, leading to total magnetic moments of 7.48 and 8.77 μ_B, respectively. These values are somewhat smaller than the theoretical value of 9 μ_B expected for a free Tb^{3+} ion. This is due to the crystalline field of the surrounding ligands which is stronger for Tb ions on site A than on site B. On site A, the most energetically preferred site of Tb is positioned in an octahedral environment, while on site B, Tb is sitting in a too large site, which creates a less intense crystalline field. This explains the weaker moment value, in particular the orbital moment of the former with respect to the latter.

Fig. 5 shows the densities of states (DOS) obtained with Tb^{3+} atoms on A and B sites computed at the DFT + U + SOC level of theory. The valence band (VB), from −12 to 0 eV, is mainly based on N 2p states interacting with Si(3p) states. The O 2p states of the interface appears in the VB from −10 to −2 eV. The conduction band, starting at 2 eV, is mainly composed of Si 3p states interacting with N 2p states. The band gap is only 2 eV in both cases. For comparison, the DFT estimated band gap of β-Si_3N_4 was 4.2 eV. The decrease in the band gap value is indeed the consequence to additional interactions involving the Tb 5d states found both at the top of the VB and the bottom of the conduction band (CB) (see Fig. 5).

Such a band gap reduction was already discussed by Huang *et al.*[40] for Y-doped Si_3N_4, due to Y 4d states. These reduced band gaps are directly responsible for the luminescent properties of the adsorbed RE-β-Si_3N_4 (RE = Eu, Tb) materials.

Mott–Schottky (MS) measurements

The emission colour of a phosphor strongly depends on the nature of the incorporated activator, the host material and its electronic configuration.[65–68] Electrochemical impedance spectroscopy (EIS) is an appropriate tool to study ion diffusion and to resolve the chemical identity of the charge carriers by the use of blocking electrodes. Mott–Schottky (MS) measurements are very sensitive to probe changes in the electronic band structure, *i.e.* charge carrier density, type of semiconducting behaviour and band edge positions, upon adsorbing. For the elucidation of the adsorbing effect on the electronic properties of Si_3N_4 and Ge_3N_4, MS measurements were conducted for the bare and RE adsorbed samples. They were performed in a 0.1 M potassium phosphate electrolyte

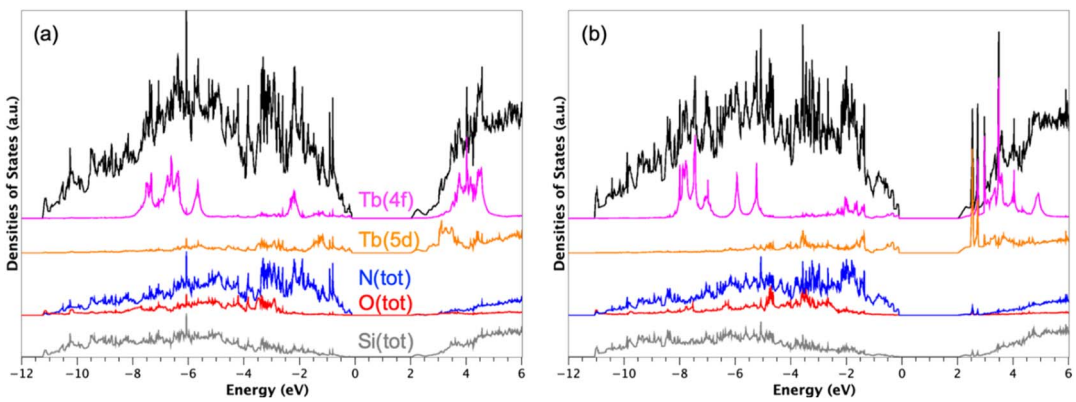

Fig. 5 Densities of states (DOS) calculated with Tb atoms on site A (a) and on site B (b). The Fermi level was defined as the reference of energies (E_F = 0 eV). The total DOS is represented in black and the projected DOS in colours. The calculations were carried out at the DFT + U + SOC level of theory, *i.e.*, with $U_{eff} = U - J$ = 6 eV for the 4f states of the rare-earth element and including spin-orbit coupling (SOC).

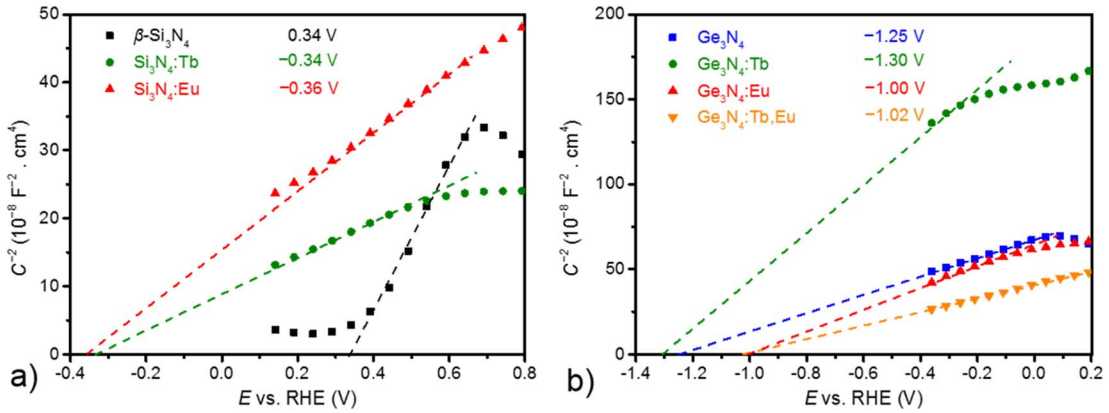

Fig. 6 MS analysis of EIS measurements of (a) pure Si_3N_4 (black), Tb-Si_3N_4 (green), Eu-Si_3N_4 (red) and (b) pure Ge_3N_4 (blue), Tb-Ge_3N_4 (green), Eu-Ge_3N_4 (red) and Eu,Tb-Ge_3N_4 (orange). Measurements were performed in a 0.1 M potassium phosphate electrolyte at pH 7, at an applied frequency of 100 Hz for (a) and an applied frequency of 1000 Hz for (b). The extrapolated curves at $y = 0$ correspond to the conduction band edges, because the materials exhibit a positive slope that is characteristic for an n-type semiconductor. The determined flatband potentials are provided in the inset.

(pH 7) in the dark with a setting at ac amplitude of 5 mV and at an applied frequency of 10 and 100 Hz (see Fig. S16 and S17†). As shown in Fig. 6, all of the acquired curves show a positive slope corresponding to the characteristic of n-type semiconductors, indicating that bare and RE adsorbed materials of β-Si_3N_4 and β-Ge_3N_4 are n-type semiconductors.[69] In addition, a smaller slope for all curves can be attributed to increased charge carrier density for Si_3N_4 upon adsorbing with the rare-earth metals.[70,71] The extrapolation of the curves allows to estimate the flat band potential as the corresponding conduction band edge of n-type semiconductors. A comparison of the results obtained from these plots in Fig. 6 reveals that the obtained conduction band edges of RE adsorbed Si_3N_4 and Ge_3N_4 yield a significant shift, indicating that RE adsorbing can be applied to modify the (photo)electrochemical properties of Si_3N_4 and Ge_3N_4.[71–73]

Conclusions

The successful adsorption of bulk β-Si_3N_4 and β-Ge_3N_4 with Eu and Tb and the synergic combination of both resulted in intriguing luminescence properties of all adsorbed compounds (red, green, orange and yellow). The theoretical and experimental results strongly highlight the opportunities for controlling functionality and luminescence properties of modern energy-efficient white light-emitting diodes.

Especially, the fact that one host can deliver different colours renders Eu,Tb-Si_3N_4 and Eu,Tb-β-Ge_3N_4 as prospective chief components for future light emitting diodes (LEDs). Not only several colours could indeed be realized by an atomic scale mixing, but the colour could also be tuned by mixing the adsorbed hosts enlarging the colour range with red, green, orange and yellow luminescence for the extremely narrow-band Eu- and Tb-M_3N_4 materials (M = Si, Ge). It could be shown that the realization of an amber emitting phosphor for both, Si_3N_4 and Ge_3N_4, is possible.

This work also studied the types and the flat band edges of β-Si_3N_4 and β-Ge_3N_4 before and after adsorption with RE materials were also studied in this work. A detailed physical characterization by MS analysis of EIS revealed that a significant shift of the flat band edge was observed caused by the adsorbing with Eu and Tb ions. This can be seen as a complementary strategy to modify the band edge of materials. Moreover, this could be applicable to photoelectrodes used to adapt and optimize (photo)electrochemical performances.

Experimental section

Adsorption of Si_3N_4 and Ge_3N_4

The adsorption of β-Si_3N_4 (Chempur 99 999%) and β-Ge_3N_4 (VWR 99 99%) was realized by a successive combustion synthesis in combination with the respective metal chlorides ($MCl_3 \cdot 6H_2O$ or $M(NO_3)_3 \cdot 5H_2O$ (M = Eu, Tb), NH_4NO_3, urea and H_2O. This mixture was put into an oven for 10 min at 400–600°. The RE content, which is about 3–5 at%, -has been checked *via* EDX measurements.

X-ray diffraction

X-ray diffraction experiments on Si_3N_4- and Ge_3N_4-based powder samples were performed on a STOE STADI P powder diffractometer in Debye–Scherrer geometry with Ge (111)-monochromatized Mo-Kα_1 radiation (λ = 0.709026 Å). The samples were enclosed in a glass capillary of 0.3 mm diameter.

EDX measurements

SEM was performed on a Zeiss Merlin microscope and for EDX we used a Quantax 400 system from Bruker.

Mott–Schottky (MS) measurements

Electrodes fabrication

Si_3N_4 and Ge_3N_4 and the corresponding rare-earth metal (RE = Eu, Tb and Eu/Tb) adsorbed semiconductor electrodes were

prepared by electrophoretic deposition. Fluorine doped tin oxide (FTO) glass (2.2 mm thick, Sigma-Aldrich) was used as the substrate after sequentially ultrasonic cleaning with dilute nitric acid, acetone and ethanol for 15 min. The dispersion was prepared by mixing 5 mg iodine and 20 mg sample with 20 ml acetone, followed by treatment with ultrasounds. The electrodes were obtained after depositing the dispersed powder at 30 V and drying under ambient atmosphere.

Mott–Schottky (MS) measurements

The MS measurements were performed in an electrochemical cell using a potentiostat (Gamry instruments) operating in a three-electrode setup. The deposited samples on FTO, a 1 M Ag/AgCl electrode and a platinum wire were used as a working electrode, a reference electrode and a counter electrode, respectively. All MS data were recorded *vs.* $E_{1\ \mathrm{M\ Ag/AgCl}}$ (V), which was subsequently converted with respect to E_{RHE} (V) according to the formula: $E_{\mathrm{RHE}}\ (\mathrm{V}) = 0.235 + E_{1\ \mathrm{M\ Ag/AgCl}} + [0.059 \times \mathrm{pH}]\ (\mathrm{V})$ at 25 °C.

Luminescence

The luminescence spectra and quantum yield measurements were performed on a Fluorolog®-3 Horiba Jobin Yvon equipped with a TBX detector picosecond photon detection device and a 450 W xenon lamp.

DFT calculations

Density functional theory (DFT) calculations were carried out on pure and adsorbed β-Si_3N_4 and β-Ge_3N_4. See ESI for the computational details.†

Author contributions

Dr Cordula Braun: concept, coordination, synthesis, luminescence investigations, writing and editing of the manuscript. Liuda Mereacre: technical help and support with synthesis investigations. D. Vincent: performed the theoretical calculations and interpreted the results. Prof. Dr X. Rocquefelte and Prof. Dr J.-F. Halet: analysed the computational data and participated to the writing and editing of the respective part of the manuscript. Prof. Dr Adam Slabon: designed the photochemical experiments (Mott–Schottky measurements) and wrote the photochemical part. Zheng Chen: performed the EIS and photochemical experiments.

Conflicts of interest

There are no conflicts of interest.

Acknowledgements

The authors gratefully acknowledge Udo Geckle (IAM-ESS KIT Karlsruhe) for the EDX and Sabine Schlabach (INT KIT Karlsruhe) for luminescence measurements. Furthermore we acknowledge support by the KIT-Publication Fund of the Karlsruhe Institute of Technology.

References

1 P. Ball, *Nat. Mater.*, 2015, **14**, 453.
2 P. Pust, P. J. Schmidt and W. Schnick, *Nat. Mater.*, 2015, **14**, 454–458.
3 S. Nakamura, *Angew. Chem., Int. Ed.*, 2015, **54**, 7770–7788.
4 I. Akasaki, *Angew. Chem., Int. Ed.*, 2015, **54**, 7750–7763.
5 H. Amano, *Angew. Chem., Int. Ed.*, 2015, **54**, 7764–7769.
6 M. Zeuner, S. Pagano and W. Schnick, *Angew. Chem., Int. Ed.*, 2011, **50**, 7754–7775.
7 H. Lange, G. Wötting and G. Winter, *Angew. Chem., Int. Ed.*, 1991, **30**, 1579–1597.
8 C. Braun, Doctoral thesis, Ludwig-Maximilians-Universität München, 2010.
9 S. R. Römer, C. Braun, O. Oeckler, P. J. Schmidt, P. Kroll and W. Schnick, *Chem.–Eur. J.*, 2008, **14**, 7892–7902.
10 T. Jüstel, H. Nikol and C. Ronda, *Angew. Chem., Int. Ed.*, 1998, **37**, 3084–3103.
11 *Luminescence*, ed. C. Ronda, Wiley-VCH Verlag GmbH & Co. KGaA, Weinheim, Germany, 2007.
12 W. Schnick, *Phys. Status Solidi*, 2009, **3**, 1–2.
13 P. Schmidt, A. Tuecks, J. Meyer, H. Bechtel, D. Wiechert, R. Mueller-Mach, G. Mueller and W. Schnick, *Seventh Int. Conf. Solid State Light.*, 2007, **6669**, P6690.
14 K. Uheda, K. Uheda, S. Shimooka, S. Shimooka, M. Mikami, M. Mikami, H. Imura, H. Imura, N. Kijima and N. Kijima, *Sci. Technol.*, 2007, 899–902.
15 L. Gamperl, P. Strobel, P. J. Schmidt and W. Schnick, *Chem.–Eur. J.*, 2022, e202200760.
16 R. Shafei, D. Maganas, P. J. Strobel, P. J. Schmidt, W. Schnick and F. Neese, *J. Am. Chem. Soc.*, 2022, **144**, 8038–8053.
17 T. De Boer, T. D. Boyko, C. Braun, W. Schnick and A. Moewes, *Int. J. Appl. Ceram. Technol.*, 2022, 1–7.
18 C. Braun, M. Seibald, S. L. Börger, O. Oeckler, T. D. Boyko, A. Moewes, G. Miehe, A. Tücks and W. Schnick, *Chem.–Eur. J.*, 2010, **16**, 9646–9657.
19 C. Braun, S. L. Börger, T. D. Boyko, G. Miehe, H. Ehrenberg, P. Höhn, A. Moewes and W. Schnick, *J. Am. Chem. Soc.*, 2011, **133**, 4307–4315.
20 C. Braun, H. Ehrenberg and W. Schnick, *Eur. J. Inorg. Chem.*, 2012, **2012**, 3923–3928.
21 R. Mueller-Mach, G. Mueller, M. R. Krames, H. A. Höppe, F. Stadler, W. Schnick, T. Juestel and P. Schmidt, *Phys. Status Solidi A*, 2005, **202**, 1727–1732.
22 Y. Q. Li, G. de With and H. T. Hintzen, *J. Mater. Chem.*, 2005, **15**, 4492–4496.
23 X. Piao, T. Horikawa, H. Hanzawa and K. Machida, *Appl. Phys. Lett.*, 2006, **88**, 161908.
24 R. J. Xie, N. Hirosaki, Y. Li and T. Takeda, *Materials*, 2010, **3**, 3777–3793.
25 R. Mueller-Mach, G. O. Mueller, M. R. Krames, O. B. Shchekin, P. J. Schmidt, H. Bechtel, C. H. Chen and O. Steigelmann, *Phys. Status Solidi*, 2009, **3**, 215–217.
26 S. Schmiechen, H. Schneider, P. Wagatha, C. Hecht, P. J. Schmidt and W. Schnick, *Chem. Mater.*, 2014, **26**, 2712–2719.

27 S. Schmiechen, P. Pust, P. J. Schmidt and W. Schnick, *Nachr. Chem.*, 2014, **62**, 847–851.
28 P. Pust, F. Hintze, C. Hecht, V. Weiler, A. Locher, D. Zitnanska, S. Harm, D. Wiechert, P. J. Schmidt and W. Schnick, *Chem. Mater.*, 2014, **26**, 6113–6119.
29 P. Pust, V. Weiler, C. Hecht, A. Tücks, A. S. Wochnik, A.-K. Henß, D. Wiechert, C. Scheu, P. J. Schmidt and W. Schnick, *Nat. Mater.*, 2014, **139**, 891–896.
30 E. Elzer, P. Strobel, V. Weiler, P. J. Schmidt and W. Schnick, *Chem. Mater.*, 2020, **32**, 6611–6617.
31 C. Braun, Bulk materials of doped multinary nitrides and nitridosilicates, their production method and uses, EP20186968, 2020.
32 C. Braun, L. Mereacre, Z. Chen and A. Slabon, *Sci. Rep.*, 2022, **12**, 1–7.
33 Y. Q. Li, N. Hirosaki, R. J. Xie, T. Takeda and M. Mitomo, *J. Lumin.*, 2010, **130**, 1147–1153.
34 Q. Li, C. Gong, X. Cheng and Y. Zhang, *Ceram. Int.*, 2015, **41**, 4227–4230.
35 Z. Huang, Z. Wang, H. Yuan, J. Zhang, F. Chen, Q. Shen and L. Zhang, *J. Mater. Sci.*, 2018, **53**, 13573–13583.
36 L.-W. Yin, Y. Bando, Y.-C. Zhu and Y.-B. Li, *Appl. Phys. Lett.*, 2003, **83**, 3584–3586.
37 R. Su, Z. F. Huang, F. Chen, Q. Shen and L. M. Zhang, *Key Engineering Materials*, Trans Tech Publications Ltd., 2017, vol. 727, pp. 635–641.
38 X. Xu, T. Nishimura, Q. Huang, R.-J. Xie, N. Hirosaki and H. Tanaka, *J. Am. Ceram. Soc.*, 2007, **90**, 4047–4049.
39 Z. Huang, F. Chen, Q. Shen and L. Zhang, *RSC Adv.*, 2016, **6**, 7568–7574.
40 Z. Huang, F. Chen, R. Su, Z. Wang, J. Li, Q. Shen and L. Zhang, *J. Alloys Compd.*, 2015, **637**, 376–381.
41 Z. Huang, R. Su, H. Yuan, J. Zhang, F. Chen, Q. Shen and L. Zhang, *Ceram. Int.*, 2018, **44**, 10858–10862.
42 N. Liu, J. Zhang, Y. Duan, X. Li and S. Dong, *J. Eur. Ceram. Soc.*, 2020, **40**, 1132–1138.
43 P. F. Becher, G. S. Painter, N. Shibata, S. B. Waters and H.-T. Lin, *J. Am. Ceram. Soc.*, 2008, **91**, 2328–2336.
44 G. S. Painter, F. W. Averill, P. F. Becher, N. Shibata, K. Van Benthem and S. J. Pennycook, *Phys. Rev. B: Condens. Matter Mater. Phys.*, 2008, **78**, 214206.
45 G. S. Painter, P. F. Becher, W. A. Shelton, R. L. Satet and M. J. Hoffmann, *Phys. Rev. B: Condens. Matter Mater. Phys.*, 2004, **70**, 144108.
46 G. S. Painter, R. L. Satet, M. J. Hoffmann, S. J. Pennycook and P. F. Becher, *Phys. Rev. B: Condens. Matter Mater. Phys.*, 2005, **72**, 140101.
47 H. Gu, X. Pan, R. M. Cannon and M. Rühle, *J. Am. Ceram. Soc.*, 1998, **81**, 3125–3135.
48 H. Hayashi, K. Hirao, M. Toriyama, S. Kanzaki and K. Itatani, *J. Am. Ceram. Soc.*, 2001, **84**, 3060–3062.
49 N. Shibata, S. J. Pennycook, T. R. Gosnell, G. S. Painter, W. A. Shelton and P. F. Becher, *Nature*, 2004, **428**, 730–733.
50 J. a. Kechele, O. Oeckler, F. Stadler and W. Schnick, *Solid State Sci.*, 2009, **11**, 537–543.
51 S. Shimooka, K. Uheda, M. Mikami, N. Kijima, H. Imura and K. Horibe, WO088966, 2007.
52 Y. Q. Li, G. De With and H. T. Hintzen, *J. Electrochem. Soc.*, 2006, **153**, G278–G282.
53 Y. Q. Li, G. de With and H. T. Hintzen, *J. Alloys Compd.*, 2004, **385**, 1–11.
54 M. J. Hoffmann, personal message, 2020.
55 C. Braun, L. Mereacre, W. Hua, T. Stürzer, I. Ponomarev, P. Kroll, A. Slabon, Z. Chen, Y. Damour, X. Rocquefelte, J. Halet and S. Indris, *ChemElectroChem*, 2020, **7**, 4550–4561.
56 D. H. Kim, J. H. Ryu and S. Y. Cho, *Appl. Phys. A: Mater. Sci. Process.*, 2011, **102**, 79–83.
57 Y. Q. Li, A. C. A. Delsing, G. De With and H. T. Hintzen, *Chem. Mater.*, 2005, **17**, 3242–3248.
58 V. Bachmann, T. Jüstel, A. Meijerink, C. Ronda and P. J. Schmidt, *J. Lumin.*, 2006, **121**, 441–449.
59 D. Halmurat, T. Yusufu, Q. Wang, J. He and A. Sidike, *Sci. Rep.*, 2019, **9**, 14637.
60 R. Mueller-Mach and G. O. Mueller, *Proc. SPIE*, 2000, **3938**, 30–41.
61 P. A. M. Berdowski, J. van Herk, L. Jansen and G. Blasse, *Phys. Status Solidi*, 1984, **125**, 387–391.
62 P. Dorenbos, *J. Mater. Chem.*, 2012, **22**, 22344–22349.
63 A. Ziegler, J. C. Idrobo, M. K. Cinibulk, C. Kisielowski, N. D. Browning and R. O. Ritchie, *Science*, 2004, **306**(5702), 1768–1770.
64 T. Mizoguchi and I. Tanaka, *Phys. Rev. B: Condens. Matter Mater. Phys.*, 2000, **61**, 2180–2187.
65 T. M. Tolhurst, P. Strobel, P. J. Schmidt, W. Schnick and A. Moewes, *Chem. Mater.*, 2017, **29**, 7976–7983.
66 M. R. Amin, P. Strobel, A. Qamar, T. Giftthaler, W. Schnick and A. Moewes, *Adv. Opt. Mater.*, 2020, **8**, 2000504.
67 T. de Boer, T. D. Boyko, C. Braun, W. Schnick and A. Moewes, *Phys. Status Solidi RRL*, 2015, **9**, 250–254.
68 M. R. Amin, E. Elzer, W. Schnick and A. Moewes, *J. Phys. Chem. C*, 2021, **125**, 11828–11837.
69 A. Lasia, in *Electrochemical Impedance Spectroscopy and Its Applications*, Springer New York, New York, NY, 2014, pp. 251–255.
70 R. O'Hayre, M. Nanu, J. Schoonman and A. Goossens, *J. Phys. Chem. C*, 2007, **111**, 4809–4814.
71 K. Gelderman, L. Lee and S. W. Donne, *J. Chem. Educ.*, 2007, **84**, 685–688.
72 B. Iandolo, H. Zhang, B. Wickman, I. Zorić, G. Conibeer and A. Hellman, *RSC Adv.*, 2015, **5**, 61021–61030.
73 D. W. Hwang, J. Kim, T. J. Park and J. S. Lee, *Catal. Lett.*, 2002, **80**, 53–57.